

Scaling in dynamical Turing pattern formation: density of defects frozen into permanent patterns

Jacek Dziarmaga

*Los Alamos National Laboratory, Theory Division T-6, MS-B288, Los Alamos, NM 87545, USA
and M.Smoluchowski Institute of Physics, Jagiellonian University, Kraków, Poland*

dziarmaga@t6-serv.lanl.gov

(February 28, 2000)

We estimate density of defects frozen into a biological Turing pattern which was turned on at a finite rate. A self-locking of gene expression in individual cells, which makes the Turing transition discontinuous, stabilizes the pattern together with its defects. A defect-free pattern can be obtained by spatially inhomogeneous activation of the genes.

Motivation and summary of results

Long time ago Turing pointed out [1] that simple reaction-diffusion (RD) systems of equations can account for formation of biological patterns. The mainstream of research, as reviewed in Ref. [2], is devoted to RD models in continuous space. The continuum RD-patterns are smooth and nonpermanent. On the other hand, it is an empirical fact that even the nearest neighbor cells can differ sharply in their biological functions and their sets of expressed genes. Moreover many biological patterns are permanent. Even the most primitive viruses, like the much studied bacteriophage λ [3], possess genetic switches that discriminate between different developmental pathways and make a once chosen pathway permanent. It is reasonable to assume that cells of higher organisms can also lock their distinctive sets of expressed genes.

The Turing patterns on figures in the review [2] are contaminated with defects. If we insist on pattern permanence, we must accept that patterns are permanent together with their defects. Sometimes, like for the animal coat patterns, permanent defects can provide an animal with its own characteristic life-long but not inheritable "fingerprints". In other cases, like formation of vital organ structures, a single defect can be fatal. In this situation it is important to understand better the origin of defects.

In this paper we use a simple toy model which in principle should give a homogeneous Turing pattern. Defects are particularly manifest on such a simple background. The model has two genes A and B . The genes are strong mutual repressors. The strong intracellular mutual inhibition is the factor responsible for pattern permanence. Both genes are activated simultaneously in a given cell when a level of their common activator a exceeds its critical value a_c . Pattern formation in RD models of Ref. [2] was simulated with fixed model parameters. In this paper we turn on the activator level a at a finite rate to find a scaling relation between density of defects and the rate. Strong mutual intracellular inhibition stabilizes the pattern together with its defects. We obtain permanent domains of A -phase and domains of B -phase divided by sharp cell-size boundaries.

We also show that an inhomogeneous activation of the genes can result in a perfect defect-free homogeneous pattern. At first the activator a exceeds a_c in a small seed area where, say, the gene A is chosen. Then a slowly spreads around gradually activating more and more cells. The initial choice of A is imposed via intercellular coupling on all newly activated cells. The inhomogeneous activation can be sufficiently characterized by a velocity v with which the critical $a = a_c$ surface spreads. Thanks to the strong mutual intracellular inhibition there is a nonzero threshold velocity v_c , such that for $v < v_c$ the formation of defects is completely suppressed. In this way the very mutual inhibition which is responsible for stability of defects can be harnessed to get rid of them.

The genetic network that we use in our toy model is functionally equivalent to the genetic toggle switch which was synthesized by the authors of the recent paper [4]. In that paper the network is studied experimentally in a single "cell". It would be interesting to generalize the experiment to a "multicellular" structure.

The toy model

For the sake of definiteness we take a genetic network with two genes A and B . A and B are mutual repressors. The network is symmetric under exchange $A \leftrightarrow B$. Expression of both genes is initiated by a common activator a . Let $A(t, \vec{x})$ and $B(t, \vec{x})$ denote time-dependent protein concentrations in the cell at the position \vec{x} . \vec{x} belongs to a discrete

square lattice with a lattice constant of 1. Evolution of the protein concentrations is described by the stochastic differential equations

$$\dot{A}(t, \vec{x}) = R S_A(t, \vec{x}) - A(t, \vec{x}) , \quad (1)$$

$$\dot{B}(t, \vec{x}) = R S_B(t, \vec{x}) - B(t, \vec{x}) . \quad (2)$$

The last terms in these equations are responsible for the protein degradation. R is a transcription rate. $S_{A,B}(t, \vec{x}) \in \{0, 1\}$ are dichotomic stochastic processes. They switch on ($0 \rightarrow 1$) and off ($1 \rightarrow 0$) transcription of a given gene. For simplicity the processes are assumed to have the same constant switch-off rate r^{off} . The switch-on rates depend on concentrations

$$r_A^{\text{on}}(t, \vec{x}) = a(t) F \left[-W B(t, \vec{x}) + V \sum_{\text{n.n. } \vec{y}} A(t, \vec{y}) \right] , \quad (3)$$

$$r_B^{\text{on}}(t, \vec{x}) = a(t) F \left[-W A(t, \vec{x}) + V \sum_{\text{n.n. } \vec{y}} B(t, \vec{y}) \right] . \quad (4)$$

W, V are positive coupling constants, $a(t)$ is a concentration of the activator. $F[z]$ is a smooth step-like sigmoidal function; the function $F[z] = 10^3 \exp(z - 2.2) / [1 + \exp(z - 2.2)]$ was used in our numerical simulations. In this model the genes A and B are mutual repressors ($W > 0$). There is a "ferromagnetic" coupling between nearest-neighbor cells ($V > 0$); expression of A in a given cell enhances expression of A in its nearest neighbors.

The model is motivated by a genetic switch between two mutual repressors like the one studied in the phage λ [3] and in the *E. coli* switch [4]. The mutual repressors have a common promoter site on DNA. A necessary condition for expression of any of them is a binding of an activator molecule to their promoter site [5]. The concentrations A and B influence its affinity to the promoter site. The gene expression is intermittent because of binding and unbinding of activator molecules. The nearest-neighbor coupling is possible thanks to signalling through intercellular membrane channels.

In an adiabatic limit, when switching of $S_{A,B}$ is much faster than protein expression and degradation, the processes $S_{A,B}$ can be replaced by their time averages,

$$\dot{A}(t, \vec{x}) = \frac{Ra(t)F \left[-W B(t, \vec{x}) + V \sum_{\text{n.n. } \vec{y}} A(t, \vec{y}) \right]}{r^{\text{off}} + a(t)F \left[-W B(t, \vec{x}) + V \sum_{\text{n.n. } \vec{y}} A(t, \vec{y}) \right]} - A(t, \vec{x}) , \quad (5)$$

$$\dot{B}(t, \vec{x}) = \frac{Ra(t)F \left[-W A(t, \vec{x}) + V \sum_{\text{n.n. } \vec{y}} B(t, \vec{y}) \right]}{r^{\text{off}} + a(t)F \left[-W A(t, \vec{x}) + V \sum_{\text{n.n. } \vec{y}} B(t, \vec{y}) \right]} - B(t, \vec{x}) . \quad (6)$$

Here we temporarily neglect any noise terms.

Attractor structure

In a subspace of uniform configurations $A(t), B(t)$ these equations simplify to the dynamical system

$$\dot{A} = \frac{RaF[-W B + 2dV A]}{r^{\text{off}} + aF[-W B + 2dV A]} - A , \quad (7)$$

$$\dot{B} = \frac{RaF[-W A + 2dV B]}{r^{\text{off}} + aF[-W A + 2dV B]} - B , \quad (8)$$

where $2d$ is the number of nearest neighbors in d dimensions.

The RHS's of these equations define a velocity field on the $A - B$ plane, which is not a gradient field. The velocity field has attractor structure which depends on the activator level a . There are two critical activator levels $a_{c_1} < a_{c_2}$. For $a < a_{c_1}$ there is one attractor at $[A, B] = [\gamma(a), \gamma(a)]$ with an increasing function $\gamma(a)$. In the range $a_{c_1} < a < a_{c_2}$ there are three attractors: the old $[\gamma(a), \gamma(a)]$ plus a new symmetric pair of $[\alpha(a), \beta(a)]$ and $[\beta(a), \alpha(a)]$ with $\alpha(a) > \beta(a)$. For $a_{c_2} < a$ there remain only the two broken symmetry attractors $[\alpha(a), \beta(a)]$ and $[\beta(a), \alpha(a)]$. The functions $\alpha(a), \beta(a)$ and $\gamma(a)$ are plotted in Fig.1.

If we start in the $[A, B] = [0, 0]$ state and slowly increase a -level, the system will stay in the $\gamma\gamma$ -phase until we reach $a = a_{c_2}$. At $a = a_{c_2}^+$ the system will roll into $\alpha\beta$ or $\beta\alpha$ -phase. On the other hand, if we start from $a_{c_2} < a$ with the system in, say, $\alpha\beta$ -phase, then we will have to decrease a down to $a = a_{c_1}$, where $\alpha\beta$ becomes unstable towards the symmetric $\gamma\gamma$ -phase. The discontinuous jumps of the concentrations are illustrated in Fig.1. This hysteresis loop is characteristic for first order phase transitions. In the adiabatic limit, where fluctuations are small, there are no short cuts via bubble nucleation. When a_{c_1} (a_{c_2}) is approached from above (below), the correlation length of small fluctuations around this uniform state diverges like in a continuous phase transition. The critical regime is narrow in the adiabatic limit so we can rely on the mean field approximation.

A finite rate Turing transition

Let us think again about starting from $[A, B] = [0, 0]$ and continuously increasing $a(t)$ above a_{c_2} . At $a_{c_2}^+$ the $\gamma\gamma$ state becomes unstable and the system has to choose between the $\alpha\beta$ and $\beta\alpha$ attractors. If $a(t)$ is increased at a finite rate, then there are finite correlated domains which make the choice independently. Despite divergence of the correlation length at $a_{c_2}^-$, the critical slowing down results in a certain finite correlation length $\hat{\xi}$ "frozen" into the fluctuations. This scale defines density of defects in the Turing pattern. This effect is well known in cosmology and condensed matter physics as Kibble-Zurek scenario [6]. In those contexts the defects disappear rapidly as a result of phase ordering kinetics. We will see that in our gene network model the defect pattern is permanent. This effect results from a combination of the hysteresis loop and the discreteness of the cell lattice.

To be more quantitative we substitute $A(t, \vec{x}) = \gamma(a(t)) + \delta A(t, \vec{x})$ and $B(t, \vec{x}) = \gamma(a(t)) + \delta B(t, \vec{x})$ into Eqs.(5) and linearize them in $\delta A, \delta B$. The linearized equations can be diagonalized by $\phi = \delta A - \delta B$ and $\psi = \delta A + \delta B$. After Fourier transformation in space

$$\phi(t, \vec{x}) = \int d^d k \tilde{\phi}(t, \vec{k}) e^{i\vec{k}\vec{x}} \quad (9)$$

they become

$$\dot{\phi}(t, \vec{k}) = R s_{\phi}(t, \vec{k}) + \frac{r^{\text{off}} R a(t) F'_a}{[r^{\text{off}} + a(t) F_a]^2} \left[W \phi(t, \vec{k}) + V e_{\vec{k}} \phi(t, \vec{k}) \right] - \phi(t, \vec{k}) \quad , \quad (10)$$

$$\dot{\psi}(t, \vec{k}) = R s_{\psi}(t, \vec{k}) + \frac{r^{\text{off}} R a(t) F'_a}{[r^{\text{off}} + a(t) F_a]^2} \left[-W \psi(t, \vec{k}) + V e_{\vec{k}} \psi(t, \vec{k}) \right] - \psi(t, \vec{k}) \quad , \quad (11)$$

where $e_{\vec{k}} = 2 \sum_{i=1}^d \cos k_i$ in d dimensions and we skipped the tildas over Fourier transforms. $F'[z] = dF[z]/dz$ and we used the shorthands $F_a^{(\prime)} = F^{(\prime)}[(-W + 2dV)\gamma(a(t))]$. $R s_{\phi, \psi}$ are noises which result from fluctuations in $R S_{A, B}$. In the adiabatic limit they can be approximated by white noises (both in space and in time) with small magnitude.

The next step is to linearize $a(t)$ around its critical value $a(t) = a_{c_2} + t/\tau$, where τ is the transition rate. This linearization gives

$$\frac{r^{\text{off}} R a(t) F'_a}{[r^{\text{off}} + a(t) F_a]^2} = c_0 + c_1 \frac{t}{\tau} + O[(t/\tau)^2] \quad . \quad (12)$$

Approximating $e_{\vec{k}} = 2d - \vec{k}^2$ in Eqs.(10,11) and keeping only leading terms in t/τ and in k^2 we get

$$\dot{\phi}(t, \vec{k}) = R s_{\phi}(t, \vec{k}) + \left[\left(\frac{c_1}{c_0} \right) \frac{t}{\tau} - (c_0 V) \vec{k}^2 \right] \phi(t, \vec{k}) \quad , \quad (13)$$

$$\dot{\psi}(t, \vec{k}) = R s_{\psi}(t, \vec{k}) - [2c_0 W + c_0 V \vec{k}^2] \psi(t, \vec{k}) \quad . \quad (14)$$

Here we used the identity $c_0[W + 2dV] = 1$, which has to be satisfied because, by definition, $\phi(t, \vec{0})$ is a zero mode at a_{c_2} . The ψ modes are stable for any \vec{k} . The ϕ -modes in the neighborhood of $\vec{k} = \vec{0}$ become unstable for $t > 0$ (or $a_{c_2} < a$). Eq.(13) is a standard linearized Landau model with the symmetry breaking parameter $(c_1/c_0)(t/\tau)$ changing sign at $t = 0$. The length scale $\hat{\xi}$ frozen into fluctuations at $t > 0$ can be estimated following the classic argument given by Zurek [6]. For $t < 0$ the model (13) has an instantaneous relaxation time $c_0\tau/c_1|t|$ and an instantaneous correlation length $c_0\sqrt{V\tau/c_1|t|}$. They both diverge at $t = 0^-$. The fluctuations can no longer follow the increasing $a(t)$ when their relaxation time becomes equal to the time still remaining to the transition at $a = a_{c_2}$, $c_0\tau/c_1|t| \approx |t|$. At this instant the correlation length is

$$\hat{\xi} \approx \left(\frac{V^{1/2} c_0^{3/4}}{c_1^{1/4}} \right) \tau^{1/4} . \quad (15)$$

This scale determines the typical size of the $\alpha\beta$ - and $\beta\alpha$ -domains. The scaling relation $\hat{\xi} \sim \tau^{1/4}$ was verified by numerical simulations illustrated at figures 2 and 3. The domain structures generated in the simulations turned out to be permanent.

The domain structures are permanent because already at a_{c_2} the width of the domain wall interpolating between $\alpha\beta$ and $\beta\alpha$ is less than the cell size (lattice spacing). The nearest neighbor cells across the wall express different genes. The width (the healing length) is determined by the longest length scale of fluctuations around the $\alpha\beta$ - or $\beta\alpha$ -state. These correlation lengths are plotted in Fig.4. For $a \geq a_{c_2}$ they are substantially less than 1. In the adiabatic limit, where the noises are weak, the domain wall cannot evolve because it would have to overcome a prohibitive potential barrier. On a cellular level the barrier originates from the mutual inhibition between A and B in a single cell. Roughly speaking, much above a_{c_1} each cell is locked in its gene expression state and insensitive to its nearest neighbors' states.

Inhomogeneous activation

The intracellular mutual inhibition stabilizes the Turing pattern but it also stabilizes the defects frozen into the pattern. With the $\hat{\xi} \sim \tau^{1/4}$ scaling the number of defects is rather weakly dependent on τ . There may be not enough time during morphogenesis to get rid of the defects by simply increasing τ . However, it is possible to generate a defect-free pattern by spatially inhomogeneous switching of the activator level a . For example, its concentration can exceed a_{c_2} at one point at first, where the cells happen to pick (or are forced to pick), say, $\alpha\beta$ -phase, and then the activator can gradually spread around so that the initial seed of $\alpha\beta$ -cells gradually imposes their choice on the whole system. For continuous transitions this effect was described in Ref. ([7]).

The effect of defect suppression in inhomogeneous activation can be most easily studied in a one dimensional version of the model (1). Suppose that a smooth activator front is moving across the one dimensional chain of cells with a velocity v , $a(t, x) \approx a_{c_2} + (vt - x)/v\tau$ close to $x = vt$ where $a = a_{c_2}$. For definiteness we impose two asymptotic conditions: for $vt \ll x$ (where $a < a_{c_2}$) the cells are in the $\gamma\gamma$ -state, and for $x \ll vt$ (where $a > a_{c_2}$) they are in $\alpha\beta$ -phase. We can expect that as the a -front moves to the right it is followed by the $\alpha\beta$ front gradually entering the area formerly occupied by the $\gamma\gamma$ -phase. If the concentration front is fast enough to move in step with the activator front, then the $\alpha\beta$ -phase will gradually fill the whole system. If, on the other hand, the concentration front is slower than the activator front then the front of the $\alpha\beta$ -phase will lag behind the $a = a_{c_2}$ front. The gap between the two fronts will grow with time. The gap will be filled with the unstable $\gamma\gamma$ -phase ($a > a_{c_2}$ behind the a -front). When the gap becomes wide enough, then $\gamma\gamma$ -state will be able to decay towards the $\beta\alpha$ -state. A domain of $\beta\alpha$ -phase will eventually be nucleated behind the a -front. Now the $\beta\alpha$ -domain will grow behind the a -front until its front lags sufficiently behind so that a new domain of $\alpha\beta$ -phase will be nucleated. In this way the activator front will leave behind a landscape of alternating $\alpha\beta$ - and $\beta\alpha$ -domains qualitatively the same as for homogeneous activation.

The success of the inhomogeneous activation depends on the relation between the velocity v of the a -front and that of the concentration front. As illustrated in Fig.4 fluctuations around the $\alpha\beta$ -state have two families of modes each with a different correlation length. For any a each \vec{k} -mode within each family has a different diffusion velocity: a ratio of its wavelength to its relaxation time. The lowest of these diffusion velocities, $v_c(a)$, is the maximal velocity at which the $\alpha\beta$ -phase can spread into the area occupied by the $\gamma\gamma$ -phase. $v_c(a_{c_2}) \equiv v_{c_2} > 0$ because at $a = a_{c_2}$ the $\alpha\beta$ -state is stable (the hysteresis loop again!). $v_c(a)$ increases with an increasing a . If $v < v_{c_2}$ the $\alpha\beta$ -front moves in step with the a -front; its tail spreads into the $vt < x$ area imposing an $\alpha\beta$ -bias on the fluctuations around $\gamma\gamma$ -state. The $\alpha\beta$ -phase spreads without nucleation of any $\beta\alpha$ -domains. For $v < v_{c_2}$ a defect-free uniform Turing pattern forms behind the activator front. Results from numerical simulations of the inhomogeneous activation are presented in Fig.5.

More complicated patterns

Finally, it is time to comment on more complicated models which are expected to give more complicated patterns than the (in principle) uniform pattern discussed so far. Let us pick a zebra pattern for example. For the uniform pattern the first mode to become unstable in Eq.(13) is the $\vec{k} = \vec{0}$ mode. The final pattern has an admixture of \vec{k} 's in a range $\approx \hat{\xi}^{-1}$ around $\vec{k} = \vec{0}$. In distinction, for the zebra pattern the first unstable modes are those on the circle $|\vec{k}| = 2\pi/L$, where L is the spacing between zebra stripes. The final pattern has an admixture of \vec{k} 's in a ring of thickness $\approx \hat{\xi}^{-1}$ around the circle $|\vec{k}| = 2\pi/L$, compare results for Swift-Hohenberg equation in Ref. [8]. This

admixture results in defects frozen into zebra pattern. The inhomogeneous activation can be applied in the zebra case too. In addition it can be used to arrange the stripes. An activator spreading from an initial point would result (at least close to the initial point) in concentric black and white rings. A front of activator moving through the system would comb the stripes perpendicular to the front.

Acknowledgements. I would like to thank M.Sadzikowski and W.Zurek for useful comments on the manuscript.

-
- [1] A.M. Turing, Phil.Trans.Roy.Soc.Lond. **B237**, 37 (1952).
 - [2] A.J. Koch and H. Meinhardt, Rev.Mod.Phys. **66**, 1481(1994).
 - [3] M. Ptashne, *A Genetic Switch: Phage and Higher Organisms*, Blackwell Science Inc. 1992; A.Arkin, J.Ross, and H.H.McAdams, Genetics **149**,1633 (1998).
 - [4] T.S.Gardner, C.R.Cantor, and J.J.Collins, Nature **403**, 339 (2000).
 - [5] M.S.H. Ko, J.Theor.Biol. **153**, 181 (1991).
 - [6] T.W.B. Kibble, Phys.Rep. **67**, 183 (1980); W.H.Zurek, Phys.Rep. **267**, 177 (1996).
 - [7] J. Dziarmaga, P.Laguna, and W.H. Zurek, Phys.Rev.Lett. **82**, 4749 (1999); N.B. Kopnin and E.V.Thuneberg, Phys.Rev.Lett. **83**, 116 (1999).
 - [8] G. Lythe, Phys.Rev.E **E53**, R4271 (1996).

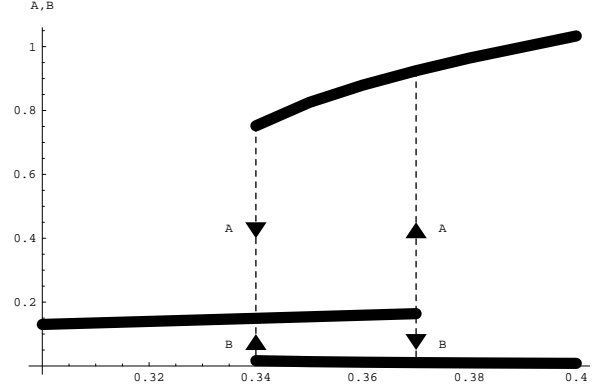


FIG. 1. The thick lines are: $\alpha(a)$ (top), $\gamma(a)$ (middle), $\beta(a)$ (bottom). The vertical lines with arrows illustrate the discontinuous jumps by the concentrations A and B during the $\alpha\beta \rightarrow \gamma\gamma$ transition at $a_{c1} \approx 0.34$, and the $\gamma\gamma \rightarrow \alpha\beta$ transition at $a_{c2} \approx 0.37$. Model parameters used in this graph are: $R = 4, W = 3, V = 1, d = 2, r^{\text{off}} = 10^3$.

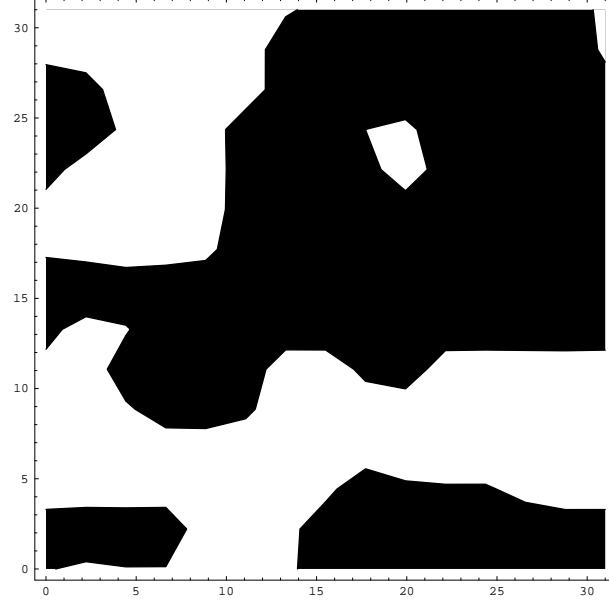


FIG. 2. Permanent pattern obtained after switching-on the activator on a 32×32 periodic lattice. It is a contour plot of $A - B$; white is A -rich ($\alpha\beta$) and black is B -rich ($\beta\alpha$). The activator was turned on as $a(t) = t/\tau$ with $\tau = 32$ and $t \in (0, 32)$. Model parameters were the same as in Fig.1. A discrete time step was $\Delta t = 10^{-4}$.

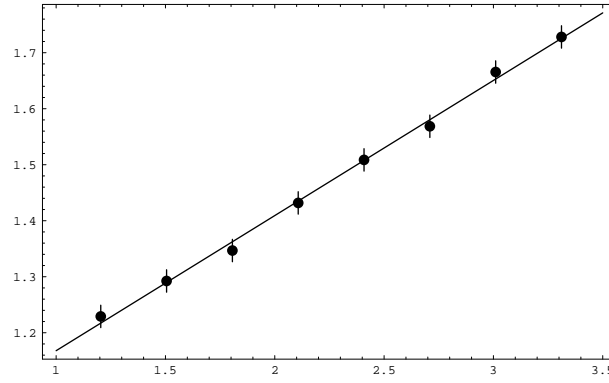


FIG. 3. $\log(\hat{\xi})$ as a function of $\log(\tau)$. $\hat{\xi}$ was obtained as an average domain size along a cross section through patterns like that in Fig.2. For any given τ the average was taken over outcomes of many simulations and over all the possible vertical and horizontal cross sections. The vertical point size is a triple standard deviation. The simulations were done on a 1024×1024 lattice. The slope was fitted as 0.24 ± 0.02 , which is consistent with the predicted 0.25.

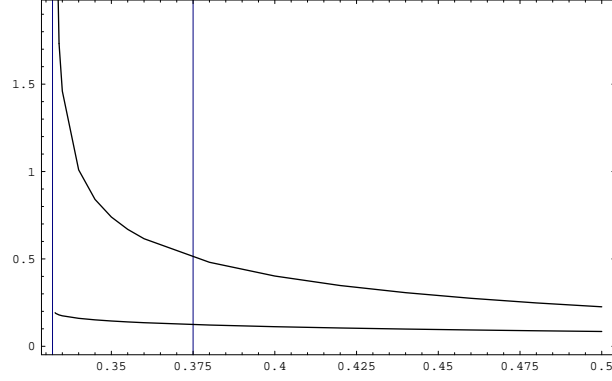


FIG. 4. The correlation lengths of the fluctuations around the state $\alpha\beta$ as functions of a . The vertical gridlines mark $a_{c_1} \approx 0.332$ and $a_{c_2} \approx 0.375$. The larger correlation length diverges at a_{c_1} . These correlation lengths should be compared with the lattice spacing which is 1. The correlation lengths were obtained by expanding $A(t, \vec{x}) = \alpha(a) + \delta A(t, \vec{x})$ and $B(t, \vec{x}) = \beta(a) + \delta B(t, \vec{x})$, Fourier-transforming the fluctuations in space and subsequent diagonalization for small k .

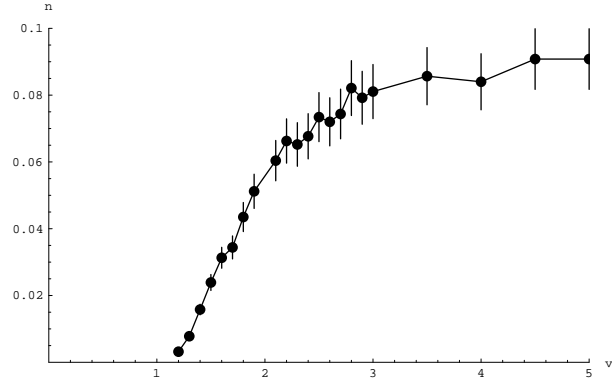


FIG. 5. Density n of domain walls between $\alpha\beta$ and $\beta\alpha$ -states behind an activator front with velocity v . The activator was $a(t, x) = (vt - x)/v\tau$ for $x < vt$ and $a(t, x) = 0$ for $vt < x$. $1/v\tau = 0.1$ was kept fixed so that the slope of a versus x was independent of v . The model parameters were the same as in Figs.1,2 but with $d = 1$ instead of 2 and $V = 2$ instead of 1 ($Vd = 2$ as before). For these model parameters $v_c \approx 0.9$ in consistency with the numerical results.